

A novel thioctic acid-functionalized hybrid network for solid-state batteries

Xuri Zuo^{a,1}, Yu Cheng^{a,1}, Lin Xu^{a,b,*}, Renpeng Chen^a, Fang Liu^a, Hong Zhang^a, Liqiang Mai^{a,b,*}



^a State Key Laboratory of Advanced Technology for Materials Synthesis and Processing, School of Materials Science and Engineering, Wuhan University of Technology, Wuhan, Hubei 430070, PR China

^b Foshan Xianhu Laboratory of the Advanced Energy Science and Technology Guangdong Laboratory, Xianhu Hydrogen Valley, Foshan, Guangdong 528200, PR China

ARTICLE INFO

Keywords:

Thioctic acid
3D cross-linked
Initiator-free polymerization
Interface
Solid-state batteries

ABSTRACT

The development of solid electrolytes for solid-state metal batteries is challenging and limited due to low ionic conductivity, poor interface stability, and accompanying side reactions. Herein, a novel thioctic acid-functionalized solid electrolyte based on hybrid heterogeneous 3D cross-linked network covalently tethering thioctic acid is designed and synthesized. Thioctic acid makes soft PEGDA polymerized in hard P(VDF-HFP) matrix to form tough hybrid heterogeneous 3D cross-linked network without initiator, which simultaneously enhances the ion transport and regulates the lithium deposition on the lithium metal surface. Moreover, the C-S bonds formed by polymerization can increase the migration rate of Li^+ , and this initiator-free polymerization process eliminates residual free radical side reactions and by-products, effectively improving the compatibility of the solid electrolyte with lithium anode. Due to the rational design, the thioctic acid-functionalized hybrid network electrolyte exhibits high ionic conductivity of 0.11 mS cm^{-1} at ambient temperature. The symmetrical Li/Li cells enable over 1800 h cycling, and the $\text{LiFePO}_4/\text{Li}$ full solid-state batteries deliver high capacity retention (>80%) over 300 cycles at 0.5 C at 25°C . This work demonstrates a rational design of thioctic acid-functionalized hybrid network with greatly improved ionic conductivity and stability for high performance solid-state batteries.

1. Introduction

Lithium metal batteries have captured worldwide attention due to their superior theoretical energy density [1,2]. However, there are many problems in traditional batteries with liquid electrolytes, including the side reaction of electrolytes with electrodes, the inevitable growth of lithium dendrites, and unstable solid electrolyte interface (SEI) [3–5]. Moreover, Lithium dendrites would pierce the separator and trigger short circuits of the battery. The flammable liquid electrolyte is prone to security accidents [5,6]. Therefore, Solid-State Batteries (SSBs) with better safety and higher energy density have been regarded as one of the most promising next-generation energy storage systems [7,8]. As for solid state electrolytes, the representative Li^+ conductors (garnet type [9], LGPS type [10], etc.) in inorganic solid electrolytes demonstrate high ionic conductivity and safety. However, the poor physical contact and relatively complicated synthesis process limit their large-scale production and application [9,10]. Solid polymer electrolytes have become the promising electrolyte materials owing to their flexibility, good interfacial contact, cost-effectiveness, and easy fabrication, but the low ionic conductivity and poor interface stability still impede their practical application [11,12]. In order to improve their ionic conductivity, organic

plasticizers (PEG [13], TEGDME [14], etc.) can be added to increase the amorphous area and reduce the crystallinity. However, the different segments mixed by conventional blending process may be inhomogeneous in phase, which cannot form the continuous Li^+ transport path [15].

To construct 3D continuous Li^+ transport path, the cross-linked electrolyte is a promising strategy that can enhance the ionic conductivity without sacrificing mechanical properties. Fan et al. designed a 3D cross-linked electrolyte through the thermal polymerization method, and it effectively enhanced the ionic conductivity of electrolyte at room temperature [16]. Jaumaux et al. proposed a safe deep eutectic solvent-based electrolyte by the thermal cross-linked polymerization, which exhibits non-combustibility, electrochemical stability, and stable interfacial properties [17]. However, most crosslinking processes use thermal or photoinitiators to generate free radicals to initiate the reaction. The residual free radicals produced by the initiators affect the interface stability between the electrode and electrolyte, causing the degradation of battery performance [18,19]. Therefore, it is indispensable to find a way to prepare a cross-linked ionic conducting network without initiators. In this regard, research efforts have been reported, such as epoxy ring-opening polymerization [20,21], thiol-ene photopolymerization [22], Electron Beam (EB) irradiation [23]. Among the various polymerization

* Corresponding authors at: State Key Laboratory of Advanced Technology for Materials Synthesis and Processing, School of Materials Science and Engineering, Wuhan University of Technology, Wuhan, Hubei 430070, PR China.

E-mail addresses: linxu@whut.edu.cn (L. Xu), mlq518@whut.edu.cn (L. Mai).

¹ These authors contributed equally to this work.

methods, radical ring-opening polymerization is attractive since it can combine heteroatoms (such as sulfide atoms) and functional groups into polymer backbone [24]. The high polarizability of thioether bonds (C-S bonds) exhibits weaker complexation with cations than ether oxygen bonds, which might be helpful for rapid cation conduction [25,26].

In this work, considering the advantages of radical ring-opening polymerization and the unique features of C-S bonds, a novel chemically stable hybrid network electrolyte was designed and synthesized via ring-opening polymerization of thiocetic acid (TA) with poly (ethylene glycol) diacrylate (PEGDA) under the framework of P(VDF-HFP). There are several unique features of our novel TA-functionalized hybrid network electrolyte. First, TA is the small biological molecule containing multiple self-polymerize reaction sites, and is linked to PEGDA and P(VDF-HFP) by covalent bonds and hydrogen bonds under heating. Second, the ether oxygen chain in PEGDA of 3D cross-linked network electrolyte can provide the strong Li^+ dissolution environment and serving as transport chains for charge carriers. Third, high polarized sulfur atoms in TA can provide suitable coordination, and thioether bonds can produce suitable sites near Li^+ transport for rapid transport. As a result, the ionic conductivity of the TA-functionalized hybrid network is increased to 0.11 mS cm^{-1} at room temperature. The 3D cross-linking heterogenous network can adjust the distribution of active sites for Li^+ deposition, thereby generating a relatively uniform deposition on the lithium surface. Furthermore, the initiator-free crosslinking process reduces the occurrence of side reactions at the interface, increasing the interface stability between the electrolyte and lithium metal. As a result, the cycle life of lithium symmetrical cells can reach 1800 h, and the $\text{LiFePO}_4/\text{Li}$ batteries exhibit superior cycle performances, indicating that the heterogenous 3D cross-linked network synthesized without initiator provide a promising way for high performance solid electrolyte.

2. Results and discussion

Fig. 1 shows the schematic of the membrane formation of the cross-linked PEGDA-TA-P(VDF-HFP) electrolyte (abbreviated as TA-hybrid network), here PEGDA and TA are inspired by vulcanization polymerized (Fig. S1). The multiple reaction sites of TA under heated conditions provide possibilities of self-polymerization and copolymerization (Fig. 1a). In 3D cross-linked structure, P(VDF-HFP) can form H-F hydrogen bonds with TA, and TA can form C-S covalent bonds with PEGDA (Fig. 1b). The addition of hard P(VDF-HFP) is beneficial for improving mechanical stability and thermal stability. Moreover, the excessive ether groups of PEGDA are hidden in the 3D cross-linked network structure to accommodate more Li^+ solvation. Photographs of TA-hybrid network in Fig. 1c show its superior flexibility. As can be seen in the FT-IR spectra for different positions of TA-hybrid network and the EDS mapping images (Figs. S2 and S3), the molecular bonding effect between PEGDA, TA, and P(VDF-HFP) offers stable and homogeneous 3D connected soft-hard polymer chains, which substantially enhances the amorphous area and flexibility of the electrolyte and supplies a better Li^+ transport path at room temperature [27].

To demonstrate the occurrence of crosslinking reaction and the morphology of products after polymerization, Scanning Electron Microscopy (SEM) is used to observe the morphology of TA-hybrid network. It reveals that a homogeneous and textured membrane is obtained after polymerization, and the wrinkled texture may be derived from the crosslinking domains between the polymer chains (Fig. 2a). A compact and well-distributed cross-sectional SEM image of TA-hybrid network is shown in Fig. 2b, indicating that the thickness of electrolyte is $\sim 50 \mu\text{m}$. The characteristics of the TA-hybrid network before and after copolymerization were characterized by Fourier Transform Infrared Spectroscopy (FT-IR). Since the double bond of PEGDA undergoes vulcanization to quench the terminal double radicals of poly (thiocetic acid), the change in the C=C bonds (Fig. 2c) peaks at about 1635 cm^{-1} indicates the occurrence of copolymerization. The Raman peaks (Fig. 2d) at 513 cm^{-1} is attributed to the vibration of disulfide bonds originated from vulcanized

PEGDA. The remarkable peak splitting at around 684 cm^{-1} indicates the existence of C-S bonds. It is reported that longer C-S bond lengths and proper coordination are conducive to segment motion, which contributes to higher ionic conductivity of solid polymer electrolyte [28].

For solid electrolytes, the crystallization changes of different components were studied by XRD. The characteristic peaks corresponding to the original crystalline P(VDF-HFP) are reduced. The TA sharp peak disappears completely (Fig. 2e), indicating that the crystallinity of the final product is reduced. To further investigate the thermal stability of the electrolyte, thermogravimetric analysis (TGA) shows that the TA-hybrid network can stand a relatively high decomposition temperature until 230°C (Fig. 2f). polymer blends have begun to lose weight around 200°C . Both electrolytes have good thermal properties, which can be attributed to the heat resistance of the P(VDF-HFP). The reason why the former is more resistant to high temperatures may be the formation of cross-linked networks.

Mechanical properties are another core parameter of solid polymer electrolytes. The high mechanical strength of the electrolyte membrane can inhibit the growth of lithium dendrites [29]. Excellent flexibility can ensure firm and stable contact between electrode and solid electrolyte during the cycle [30]. The crosslinking 3D network improves the toughness of the film and ensures good flexibility. Fig. S4 presents the strain-stress curves of the TA-hybrid network and polymer blends at room temperature. The enhanced tensile strength of the TA-hybrid network is 1.53 MPa with an elongation-at-break of 330% with the addition of cross-linking agents. In contrast, the performance of polymer blends is relatively poor since no cross-linking reaction occurs.

The ionic conductivity is an important index for evaluating solid electrolyte. By testing the impedance of TA-hybrid network (Fig. 3a) and polymer blends (Fig. S5) at different temperatures. The TA-hybrid network electrolyte shows a prominent high ionic conductivity value (0.11 mS cm^{-1}) at ambient temperature (Fig. S6), which is seven times higher than polymer blends (Table S1). Fig. S7 shows the temperature dependence of the ionic conductivity of TA-hybrid network electrolytes membranes in the temperature range of $20\text{--}80^\circ\text{C}$. The corresponding Arrhenius plots are depicted in Fig. 3b, and the TA-hybrid network reveals a more stable temperature-dependent conductivity with lower activation energy (E_a) of 0.21 eV whereas 0.37 eV of polymer blends, which matches well with the high ionic conductivity. The increase in ionic conductivity may be attributed to the synergistic effect of weak coordination of thioether bonds and the 3D cross-linked Li^+ conductive network paths [25,31]. The electrochemical stabilities of electrolyte were tested by linear sweep voltammetry (LSV) in Fig. 3c. Compared to the polymer blends of $4.1 \text{ V vs. Li}^+/\text{Li}$, the TA-hybrid network exhibits improved anodic stability, and no decomposition occurs below $4.3 \text{ V vs. Li}^+/\text{Li}$. The Li^+ transference number (LITN) is another important aspect of electrolytes to reflect the ratio of mobile Li^+ . The LITN of the TA-hybrid network was calculated to be 0.47 (Fig. 3d), because TA can weaken the coordination between Li^+ and -EO- unit on the PEGDA segment and facilitate the separation of Li^+ from ion pairs. For another, the cross-linked network formed by the self-polymerization and copolymerization of TA impedes the movement of anions [14], thus retards Li dendrite nucleation and effectively blocks the growth of Li dendrites [32].

The symmetrical Li cells are applied for the galvanostatic cycling test to observe the interfacial stability in the process of lithium-ion stripping/plating. The TA-hybrid network exhibits a relatively steady cycling performance in $\text{Li/TA-hybrid network/Li}$ at 0.1 mA cm^{-2} for 1800 h (Fig. 4a) due to good compatibility between the TA-hybrid network and lithium metal, indicating a certain resistance to the growth of lithium dendrites [33]. As shown in Fig. 4b, under different current densities of $0.05, 0.1, 0.2, 0.3$, and 0.4 mA cm^{-2} , after 10 h cycling, the $\text{Li/TA-hybrid network/Li}$ symmetrical cells exhibit stable lithium electroplating/dissolution, and the polarization voltage is $15, 30, 60, 95, 140 \text{ mV}$, respectively. Moreover, at a constant capacity of 0.2 mAh cm^{-2} , the symmetrical cell tests under current densities of $0.1, 0.2, 0.4$,

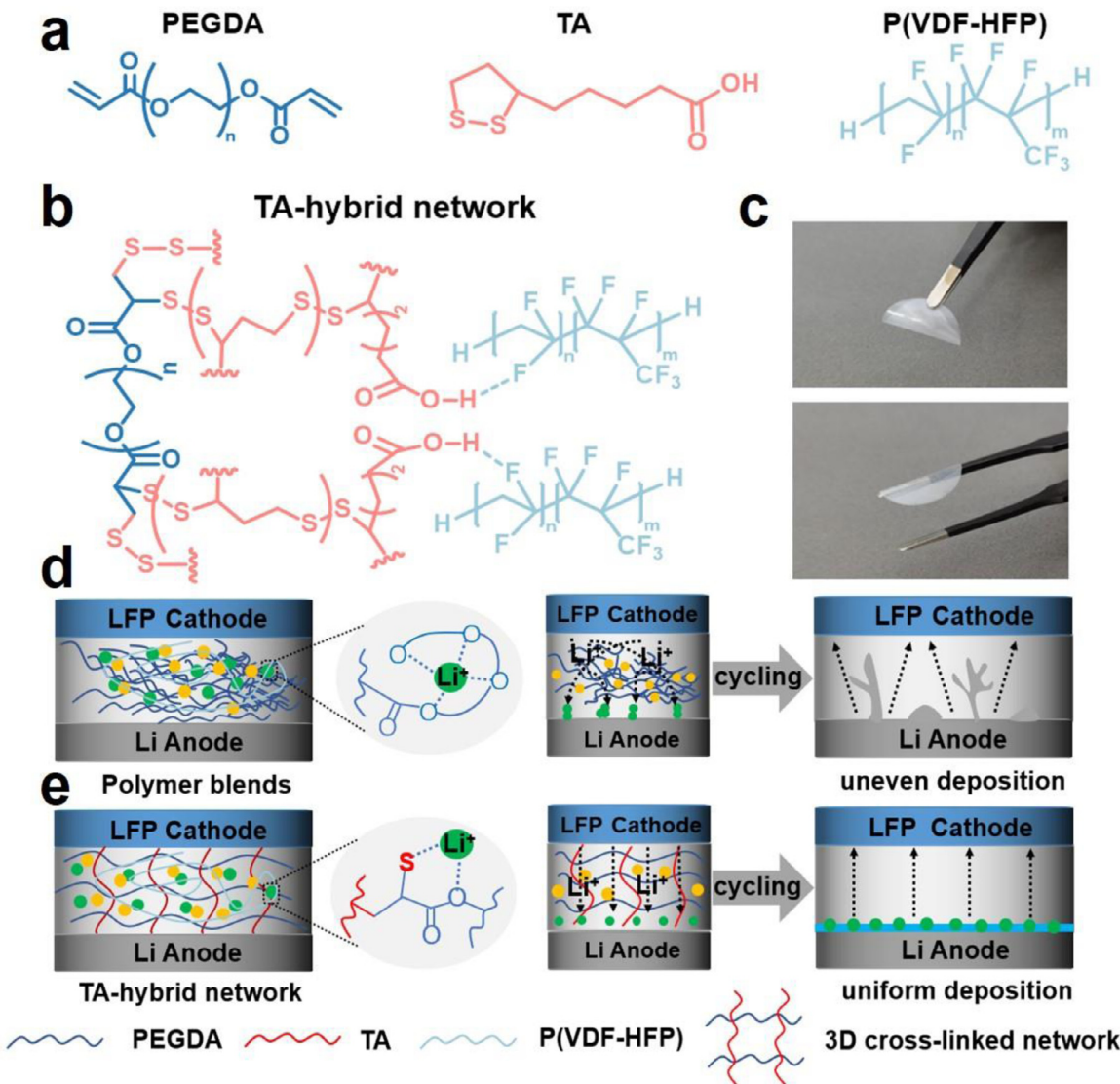


Fig. 1. (a) Chemical structures for PEGDA, TA and P(VDF-HFP). (b) Schematic illustration of the prepared TA-hybrid network structure and the intermolecular hydrogen binding effect. (c) Photographs for TA-hybrid network. Schematic illustration of the superiority of 3D cross-linked network that works in solid-state lithium batteries. (d) Li-ion transport pathways in polymer blends. (e) Li-ion transport pathways in TA-hybrid network.

and 0.5 mA cm^{-2} in Fig. S8 show ultralow overpotentials. Remarkably, at a relatively high current density of 0.5 mA cm^{-2} , the cell maintains an overpotential value of 150 mV . However, the polarization voltage of the polymer blends symmetrical battery rises greatly with the cycle time increases, even more than 750 mV (Fig. S9). In comparison, the TA-hybrid network is more conducive to Li^+ transport and has a smaller polarization. The morphology of lithium electrode surface was detected. A pulverized rough surface is observed on the lithium electrode retrieved from cells after 100 cycles with the polymer blends (Fig. 4c), while the TA-hybrid network is used as an electrolyte to assemble a symmetrical cell under the same conditions, and the surface of the lithium sheet after cycling is smooth without obvious cracks and pits (Fig. 4d). The results demonstrate that an intimate interfacial contact is generated by the formed 3D cross-linked network, which enables lithium ions to deposit uniformly on the lithium anode surface.

Fig. 4e shows the EIS impedance spectrum of the Li/TA-hybrid network/Li cell after cycle. The equivalent circuit models for fitting the Nyquist diagrams are shown in Fig. S10. The impedance spectrum curves can be divided into two parts: the intersection of the curve with the real axis at high frequency region (resistance in the bulk of SPE, R_s) and the

intermediate frequency semicircle (including the reaction resistance at the electrolyte/electrode interface, R_{int}) [13]. In Fig. 4e, the decrease in R_s is due to increased contact at the electrolyte interface, but remains almost unchanged during subsequent cycles, indicating that the cell is stable thereafter [34,35]. The Li/TA-hybrid network/Li cell shows an initial R_{int} of $\sim 750 \Omega$, which is then reduced to $\sim 100 \Omega$ after 10 cycles. Thereafter, the R_{int} of the Li//Li cell increase gradually with the cycle number increase. Even though, after 50 cycles, the surface impedance remained as low as 400Ω , showing that TA-hybrid network has good compatibility with the Li-metal anode. Moreover, the composition of SEI layer in the cycle of Li//Li battery was investigated by X-ray Photoelectron Spectroscopy (XPS) (Fig. 4f-i). As shown in F1s spectra, it can be seen that more LiF is formed on the lithium metal surface in contact with the TA-hybrid network electrolyte (Fig. 4g and i). It is reported the presence of LiF-rich SEI can probably yield great ascendancy associated with regulating homogeneous deposition of Li^+ ions flux [36,37]. Moreover, the distinct difference between the two samples can be found in the C1s spectra. Two extra peaks centered at 290.8 eV and 292.8 eV occurs for the SEI formed in the polymer blends, whereas these two peaks do not show up in the SEI formed with TA-hybrid network. This peak

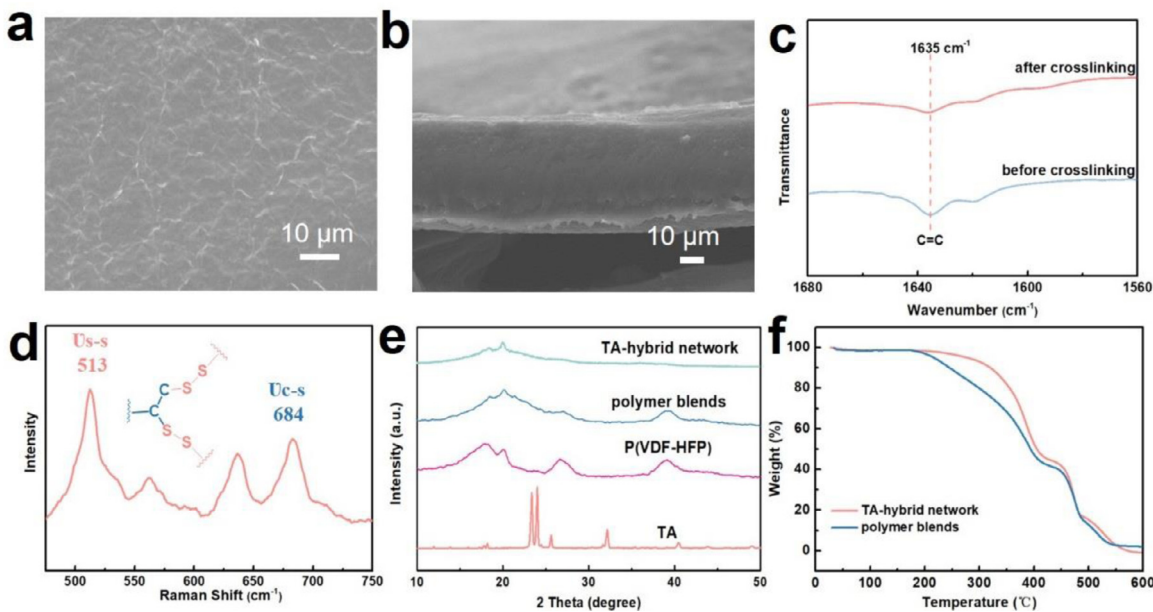


Fig. 2. (a) Top-view and (b) Cross-sectional SEM images of the TA-hybrid network. (c) FT-IR spectra of the TA-hybrid network (before/after crosslinking). (d) Raman spectrum of the TA-hybrid network. (e) XRD patterns. (f) TGA thermograms of the TA-hybrid network and polymer blends.

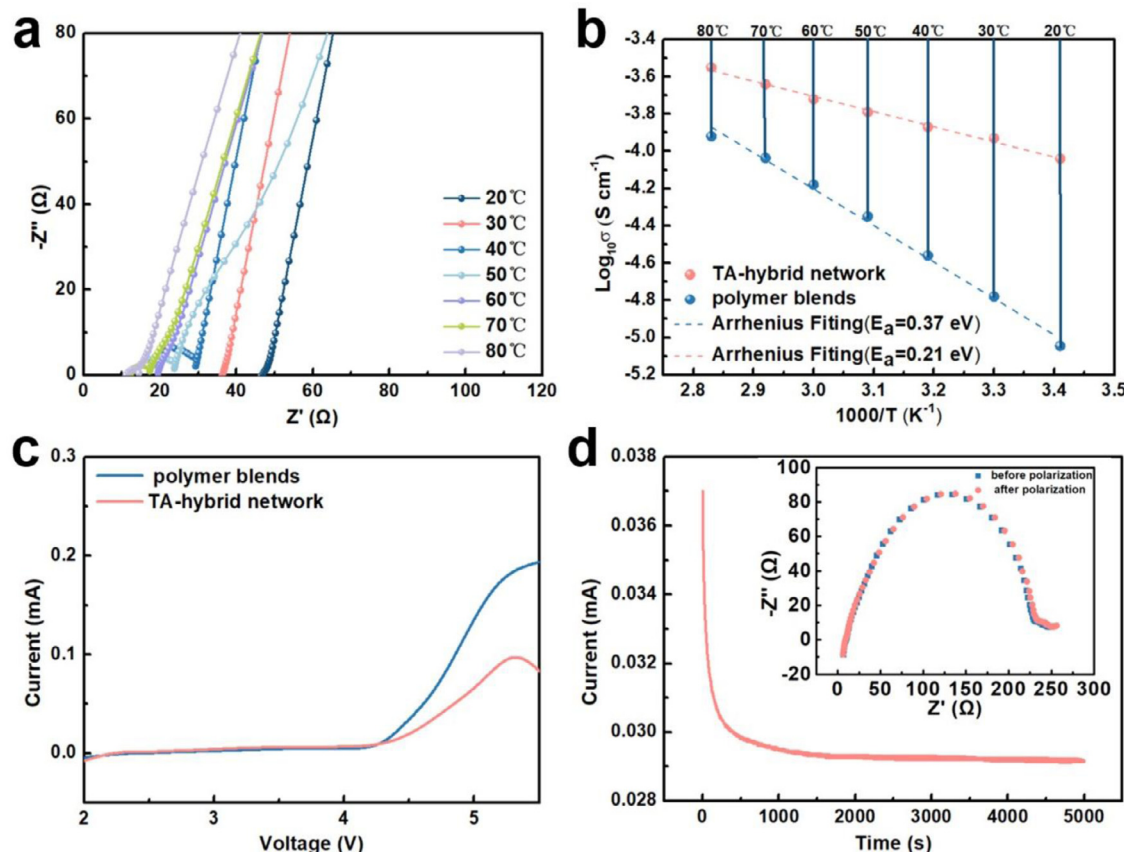


Fig. 3. (a) EIS curves of TA-hybrid network from 20 to 80 °C. (b) Ionic conductivities of TA-hybrid network (red point) and polymer blends (blue point) as a function of temperature. The plots represent the experimental data meanwhile the dotted lines represent Arrhenius fitting results. (c) LSV of the TA-hybrid network and polymer blends at a scan rate of 10 mV s⁻¹ using stainless steel as working electrode, and Li as counter and reference electrodes. (d) Current-time profiles of the Li/TA-hybrid network/Li symmetrical batteries after applying a DC voltage of 10 mV on the batteries. The inset shows the Nyquist impedance spectra of the batteries before and after polarization.

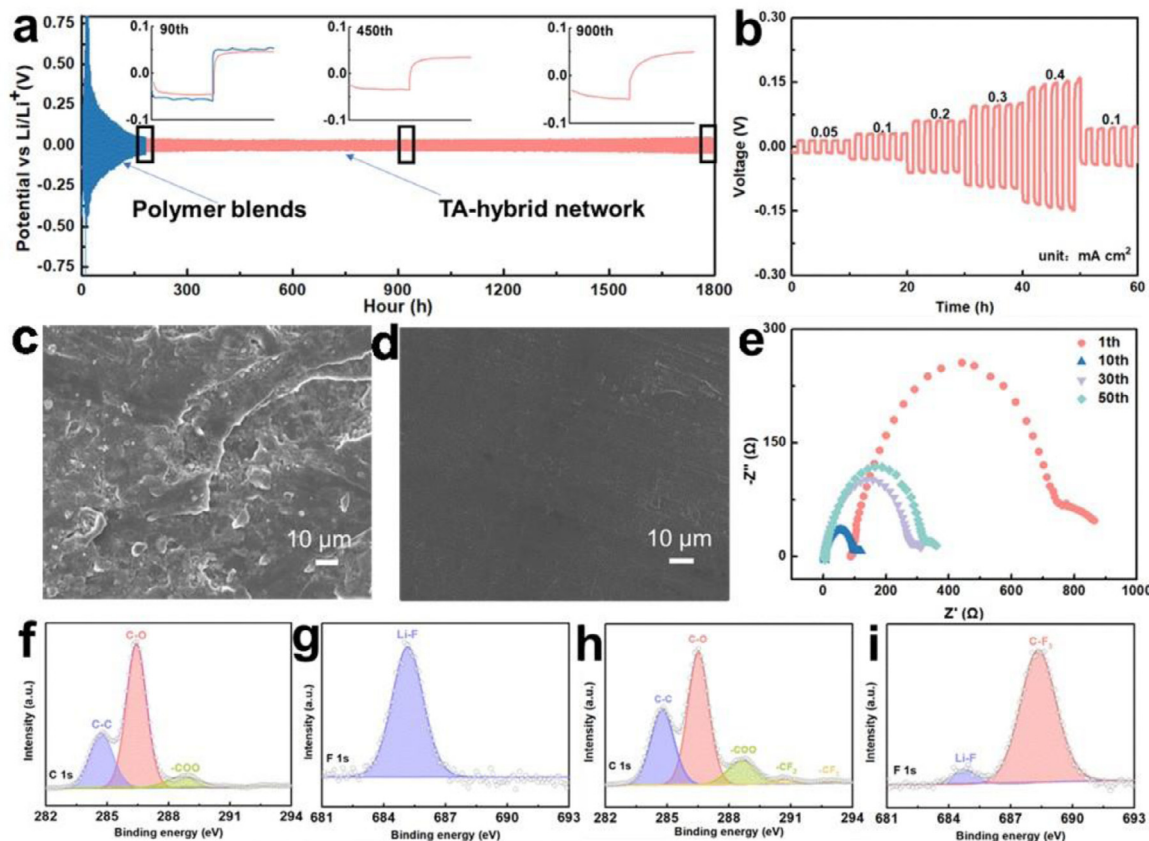


Fig. 4. (a) Li//Li symmetric cells with TA-hybrid network at a current density of 0.1 mA cm^{-2} with a capacity of 0.1 mAh cm^{-2} at 25°C . Insets: voltage profiles at 90th, 450th, and 900th cycles of the Li/TA-hybrid network/Li cell. (b) Voltage profile of the lithium plating/stripping cycling in the symmetrical Li/TA-hybrid network/Li cell with different current densities of $0.05, 0.1, 0.2, 0.3$ and 0.4 mA cm^{-2} , respectively. SEM images of Li metal surface in (c) Li/polymer blends/Li and in (d) Li/TA-hybrid network/Li after cycling. (e) Alternating current impedance profiles of Li/TA-hybrid network/Li at different cycles. X-ray photoelectron spectroscopy spectra of interface of Li foils after cycling with the TA-hybrid network (900th cycle) and polymer blends (90th cycle). (f) C 1s and (g) F 1s of TA-hybrid network on the Li anode side. (h) C 1s and (i) F 1s of polymer blends on the Li anode side.

can be assigned to C in the functional group $-\text{CF}_2$ and $-\text{CF}_3$, which may originate from $\text{Li}_2\text{NSO}_2\text{CF}_3$ and LiCF_3 [38,39]. These two compounds are the products of LITFSI decomposition [40], which proves that the TA-hybrid network electrolyte is beneficial to stable SEI and reduces the source of interfacial by-products.

Full battery tests are the most comprehensive evaluation of all aspects of electrolyte performance. To demonstrate the applications, the solid-state lithium batteries (SSLBs) composed of LiFePO_4 as cathode, TA-hybrid network or polymer blends as electrolytes and Li metal as anode were assembled. At a rate of 0.5 C under ambient temperature, the cycling stabilities of solid-state batteries assembled with TA-hybrid network and polymer blends were compared in Fig. 5a. The batteries using TA-hybrid network deliver a maximum specific capacity of 140.2 mAh g^{-1} and remain 136.1 mAh g^{-1} after 150 cycles, corresponding to a capacity retention of 97%. Conversely, although the discharge capacity of battery assembled with polymer blends is equal to that of TA-hybrid network at the beginning, the decreasing of the battery's capacity is very noticeable, the final capacity is only 50.1 mAh g^{-1} after 150 cycles. Meanwhile, a comparison between this work and previously reported SSLBs in terms of capacity retention in different conditions is shown (Table S2). The stable cycling performance of TA-hybrid network can be attributed to 3D rapid Li^+ transport paths and enhanced Li anode compatibility.

Fig. 5b illustrates the rate performances of Li/TA-hybrid network/LFP batteries at room temperature, as the current density rise, the discharge voltage value decreases slowly. The discharge capacity is 156.6 mAh g^{-1} at 0.1 C , approximately 92.1% of the theoretical ca-

pacity of LiFePO_4 (170 mAh g^{-1}). The batteries deliver high reversible capacities of 152.4 mAh g^{-1} at 0.2 C and 143.2 mAh g^{-1} at 0.5 C . When the rate is restored to 0.1 C , the specific capacity quickly returns to 156.3 mAh g^{-1} . Corresponding discharge-charge curves is shown in Fig. 5c, remarkably, at a relatively high discharge/charge rate of 1 C , the cell maintains a high capacity of 134.5 mAh g^{-1} , over-potential value is as low as 0.06 V at 0.1 C . However, the specific capacities of Li/polymer blends/LFP cells were only 132.2 mAh g^{-1} , 129.1 mAh g^{-1} , 122.1 mAh g^{-1} , and 107.4 mAh g^{-1} when cycling at 0.1 C , 0.2 C , 0.5 C , and 1 C , respectively, much lower than that of the Li/TA-hybrid network/LFP cell. These results demonstrate that compared to the polymer blends, the 3D continuous Li^+ transport path with thioether bonds in the TA-hybrid network possessed higher ionic conductivity and excellent interface stability, and contributed to the significantly enhanced performance of LFP//Li batteries. Additionally, the LFP/TA-hybrid network/Li pouch cell was assembled to verify the practicality of different conditions. As illustrated in Fig. 5d-f, the pouch cell initially exhibits high open-circuit voltages and it proves the same ability to lighting Light-emitting diode (LED) devices before and after folding testing. Even shortly after several cutting, the pouch cell can still successfully light up the green LED (Fig. 5g), which indicates that the TA-hybrid network solid electrolyte can be used to produce flexible solid state batteries with high safety.

Our designed TA-functionalized polymer electrolyte greatly affects the process of lithium deposition behavior. In the polymer blends system (like traditional polymer electrolytes), brief blending of PEGDA and P(VDF-HFP) does not form a 3D cross-linked network. The coordination sites of lithium ions between polymer chains are randomly distributed

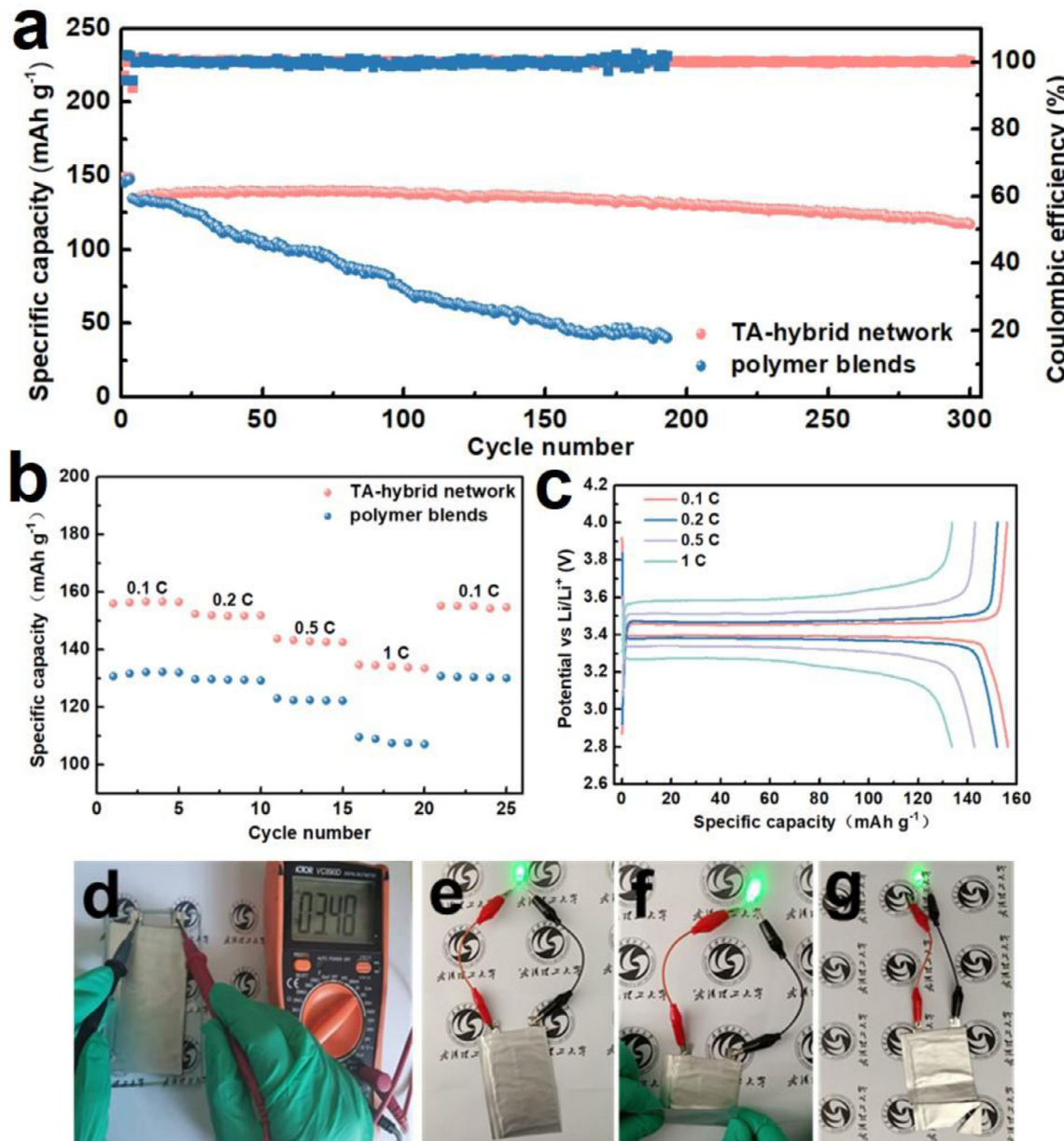


Fig. 5. Electrochemical performances of Li/TA-hybrid network/LFP cell at room temperature. (a) Cycling performances. (b) Rate performance of solid-state batteries with TA-hybrid network, and polymer blends, respectively. (c) typical charge-discharge profiles of Li/TA-hybrid network/LFP. (d) Photographs of the open-circuit voltage of pouch cell with the construction of Li/TA-hybrid network/LFP and the green LED lit up under various extreme conditions, (e) unfolding, (f) folding, and (g) snipping.

at the interface (Fig. 1d). The developed active areas are unevenly distributed. Li⁺ preferentially accumulates and deposits at sites with higher active sites to form dendrites, thus lithium is not uniformly deposited during the discharge process to produce a new SEI layer or even dead lithium [41,42]. On the contrary, the 3D cross-linking network is introduced to effectively adjust the distribution of coordination sites in TA-hybrid network, resulting in a relatively uniform interface deposition site (Fig. 1e). In addition, the thioether bonds and the coordination of the ether oxygen segments synergistically ensure continuous Li⁺ transfer channels in the electrolyte system.

3. Conclusion

In summary, we designed a novel thioctic acid-functionalized polymer electrolyte under initiator-free that can simultaneously possess high

ionic conductivity, stable interfacial and dendrite-free Li plating. The effect of thioctic acid-functionalized includes the synergistic impact of highly polarized sulfur atom polymer and ether oxygen segment, which accelerates the dissociation of lithium salt while providing a good transport path for lithium ions. The formation of the 3D cross-linked network regulates the distribution of active sites for lithium deposition at the interface, leading to a more relatively uniform lithium deposition process. Moreover, compared with the initiators for cross-linked polymerization, the advantages of the polymerization methods reported here are its mild reaction conditions and ease of control. It is free of by-product that deteriorates battery performance caused by initiators. These exceptional features ensure satisfactory cycling performances when applying the TA-hybrid network in symmetrical Li//Li and Li//LFP batteries. This simple initiators-free synthesis method and favorable performance make it possible for other battery systems.

Declaration of Competing Interest

The authors declare no conflict of interest.

CRediT authorship contribution statement

Xuri Zuo: Conceptualization, Methodology, Investigation, Data curation, Visualization, Writing – original draft, Writing – review & editing. **Yu Cheng:** Conceptualization, Data curation, Writing – review & editing. **Lin Xu:** Conceptualization, Writing – review & editing, Supervision, Funding acquisition, Project administration, Resources. **Renpeng Chen:** Writing – review & editing. **Fang Liu:** Writing – review & editing. **Hong Zhang:** Writing – review & editing. **Liqiang Mai:** Conceptualization, Writing – review & editing, Supervision, Funding acquisition, Project administration, Resources.

Acknowledgment

This work was supported by the National Key Research and Development Program of China (2020YFA0715000), National Natural Science Foundation of China (Grant No: 51802239, 52127816), the Key Research and Development Program of Hubei Province (2021BAA070), Foshan Xianhu Laboratory of the Advanced Energy Science and Technology Guangdong Laboratory (Grant No. XHT2020–005), and the Fundamental Research Funds for the Central Universities (Grant Nos. WUT: 2020III011GX, 2020IVB057, 2019IVB054, 2019III062JL).

Supplementary materials

Supplementary material associated with this article can be found, in the online version, at doi:[10.1016/j.ensm.2022.01.045](https://doi.org/10.1016/j.ensm.2022.01.045).

References

- [1] W. Xu, J.L. Wang, F. Ding, X.L. Chen, E. Nasybutin, Y.H. Zhang, J.G. Zhang, Lithium metal anodes for rechargeable batteries, *Energy Environ. Sci.* 7 (2014) 513–537.
- [2] D. Lin, Y. Liu, Y. Cui, Reviving the lithium metal anode for high-energy batteries, *Nat. Nanotechnol.* 12 (2017) 194–206.
- [3] F. Ding, W. Xu, X. Chen, J. Zhang, M.H. Engelhard, Y. Zhang, B.R. Johnson, J.V. Crum, T.A. Blake, X. Liu, J.G. Zhang, Effects of carbonate solvents and lithium salts on morphology and coulombic efficiency of lithium electrode, *J. Electrochem. Soc.* 160 (2013) A1894–A1901.
- [4] K.B. Hatzell, X.C. Chen, C.L. Cobb, N.P. Dasgupta, M.B. Dixit, L.E. Marbella, M.T. McDowell, P.P. Mukherjee, A. Verma, V. Viswanathan, A.S. Westover, W.G. Zeier, Challenges in lithium metal anodes for solid-state batteries, *ACS Energy Lett.* 5 (2020) 922–934.
- [5] K. Xu, Nonaqueous liquid electrolytes for lithium-based rechargeable batteries, *Chem. Rev.* 104 (2004) 4303–4417.
- [6] K. Amine, R. Kanoo, Y. Tzeng, Rechargeable lithium batteries and beyond: progress, challenges, and future directions, *MRS Bull.* 39 (2014) 395–401.
- [7] A. Manthiram, X. Yu, S. Wang, Lithium battery chemistries enabled by solid-state electrolytes, *Nat. Rev. Mater.* 2 (2017) 16103.
- [8] Q. Zhao, S. Stalin, C.Z. Zhao, L.A. Archer, Designing solid-state electrolytes for safe, energy-dense batteries, *Nat. Rev. Mater.* 5 (2020) 229–252.
- [9] T. Famprakis, P. Canepa, J.A. Dawson, M.S. Islam, C. Masquelier, Fundamentals of inorganic solid-state electrolytes for batteries, *Nat. Mater.* 18 (2019) 1278–1291.
- [10] F. Liang, Y. Sun, Y. Yuan, J. Huang, M. Hou, J. Lu, Designing inorganic electrolytes for solid-state Li-ion batteries: a perspective of LGPS and garnet, *Mater. Today* 50 (2021) 418–441.
- [11] J. Li, Y. Cai, H. Wu, Z. Yu, X. Yan, Q. Zhang, T.Z. Gao, K. Liu, X. Jia, Z. Bao, Polymers in lithium-ion and lithium metal batteries, *Adv. Energy Mater.* 11 (2021) 2003239.
- [12] Q. Zhang, K. Liu, F. Ding, X. Liu, Recent advances in solid polymer electrolytes for lithium batteries, *Nano Res.* 10 (2017) 4139–4174.
- [13] Y. Zhang, W. Lu, L. Cong, J. Liu, L. Sun, A. Mauger, C.M. Julien, H. Xie, J. Liu, Cross-linking network based on poly (ethylene oxide): solid polymer electrolyte for room temperature lithium battery, *J. Power Sources* 420 (2019) 63–72.
- [14] F. Fu, W. Lu, Y. Zheng, K. Chen, C. Sun, L. Cong, Y. Liu, H. Xie, L. Sun, Regulating lithium deposition via bifunctional regular-random cross-linking network solid polymer electrolyte for Li metal batteries, *J. Power Sources* 484 (2021) 229186.
- [15] D. Lin, W. Liu, Y. Liu, H.R. Lee, P.C. Hsu, K. Liu, Y. Cui, High ionic conductivity of composite solid polymer electrolyte via *in situ* synthesis of monodispersed SiO₂ nanospheres in poly (ethylene oxide), *Nano Lett.* 16 (2016) 459–465.
- [16] W. Fan, N.W. Li, X. Zhang, S. Zhao, R. Cao, Y. Yin, Y. Xing, J. Wang, Y.G. Guo, C. Li, A dual-salt gel polymer electrolyte with 3D cross-linked polymer network for dendrite-free lithium metal batteries, *Adv. Sci.* 5 (2018) 1800559.
- [17] P. Jaumaux, Q. Liu, D. Zhou, X. Xu, T. Wang, Y. Wang, F. Kang, B. Li, G. Wang, Deep-eutectic-solvent-based self-healing polymer electrolyte for safe and long-life lithium-metal batteries, *Angew. Chem. Int. Ed.* 59 (2020) 9134–9142.
- [18] Q. Lu, Y.B. He, Q. Yu, B. Li, Y.V. Kaneti, Y. Yao, F. Kang, Q.H. Yang, Dendrite-free, high-rate, long-life lithium metal batteries with a 3D cross-linked network polymer electrolyte, *Adv. Mater.* 29 (2017) 1604460.
- [19] Y. Cui, X. Liang, J. Chai, Z. Cui, Q. Wang, W. He, X. Liu, Z. Liu, G. Cui, J. Feng, High performance solid polymer electrolytes for rechargeable batteries: a self-catalyzed strategy toward facile synthesis, *Adv. Sci.* 4 (2017) 1700174.
- [20] Z. Zeng, X. Chen, M. Sun, Z. Jiang, W. Hu, C. Yu, S. Cheng, J. Xie, Nanophase-separated, elastic epoxy composite thin film as an electrolyte for stable lithium metal batteries, *Nano Lett.* 21 (2021) 3611–3618.
- [21] Y. Zhu, J. Cao, H. Chen, Q. Yu, B. Li, High electrochemical stability of a 3D cross-linked network PEO@nano-SiO₂ composite polymer electrolyte for lithium metal batteries, *J. Mater. Chem. A* 7 (2019) 6832–6839.
- [22] C. Zuo, B. Zhou, Y.H. Jo, S. Li, G. Chen, S. Li, W. Luo, D. He, X. Zhou, Z. Xue, Facile fabrication of a hybrid polymer electrolyte via initiator-free thiol-ene photopolymerization for high-performance all-solid-state lithium metal batteries, *Polym. Chem.* 11 (2020) 2732–2739.
- [23] M. Ueno, N. Imanishi, K. Hanai, T. Kobayashi, A. Hirano, O. Yamamoto, Y. Takeda, Electrochemical properties of cross-linked polymer electrolyte by electron beam irradiation and application to lithium ion batteries, *J. Power Sources* 196 (2011) 4756–4761.
- [24] A. Tardy, J. Nicolas, D. Gigmes, C. Lefay, Y. Guillaneuf, Radical ring-opening polymerization: scope, limitations, and application to (bio) degradable materials, *Chem. Rev.* 117 (2017) 1319–1406.
- [25] J.M. Sarapas, G.N. Tew, Poly(ether-thioethers) by thiol-ene click and their oxidized analogues as lithium polymer electrolytes, *Macromolecules* 49 (2016) 1154–1162.
- [26] K. Takada, Progress and prospective of solid-state lithium batteries, *Acta Mater.* 61 (2013) 759–770.
- [27] G. Chen, F. Zhang, Z. Zhou, J. Li, Y. Tang, A flexible dual-ion battery based on PVDF-HFP-modified gel polymer electrolyte with excellent cycling performance and superior rate capability, *Adv. Energy Mater.* 8 (2018) 1801219.
- [28] C. Xuan, S. Gao, Y. Wang, Q. You, X. Liu, J. Liu, R. Xu, K. Yang, S. Cheng, Z. Liu, Q. Guo, *In-situ* generation of high performance thiol-conjugated solid polymer electrolytes via reliable thiol-acrylate click chemistry, *J. Power Sources* 456 (2020) 228024.
- [29] D.G. Mackanic, X. Yan, Q. Zhang, N. Matsuhisa, Z. Yu, Y. Jiang, T. Manika, J. Lopez, H. Yan, K. Liu, X. Chen, Y. Cui, Z. Bao, Decoupling of mechanical properties and ionic conductivity in supramolecular lithium ion conductors, *Nat. Commun.* 10 (2019) 5384–5395.
- [30] J.R. Nair, M. Destro, F. Bella, G.B. Appeteccchi, C. Gerbaldi, Thermally cured semi-interpenetrating electrolyte networks (s-ipn) for safe and aging-resistant secondary lithium polymer batteries, *J. Power Sources* 306 (2016) 258–267.
- [31] D. Xu, J. Jin, C. Chen, Z. Wen, From nature to energy storage: a novel sustainable 3D cross-linked chitosan-peptide-based gel polymer electrolyte with excellent lithium-ion transport properties for lithium batteries, *ACS Appl. Mater. Interfaces* 10 (2018) 38526–38537.
- [32] X.B. Cheng, Q. Zhang, Dendrite-free lithium metal anodes: stable solid electrolyte interphases for high-efficiency batteries, *J. Mater. Chem. A* 3 (2015) 7207–7209.
- [33] S.S. Chi, Y. Liu, N. Zhao, X. Guo, C.W. Nan, L.Z. Fan, Solid polymer electrolyte soft interface layer with 3D lithium anode for all-solid-state lithium batteries, *Energy Storage Mater.* 17 (2019) 309–316.
- [34] S. Liu, Y. Zhao, X. Li, J. Yu, J. Yan, B. Ding, Solid-state lithium metal batteries with extended cycling enabled by dynamic adaptive solid-state interfaces, *Adv. Mater.* 12 (2021) e2008084.
- [35] W. Li, J. Gao, H. Tian, X. Li, S. He, J. Li, W. Wang, L. Li, H. Li, J.S. Qiu, W.D. Zhou, SnF₂-catalyzed formation of polymerized dioxolane as solid electrolyte and its thermal decomposition behavior, *Angew. Chem. Int. Ed.* 61 (2021) e202114805.
- [36] Y.Y. Lu, Z. Tu, L.A. Archer, Stable lithium electrodeposition in liquid and nanoporous solid electrolytes, *Nat. Mater.* 13 (2014) 961–969.
- [37] J. Tan, J. Matz, P. Dong, J. Shen, M. Ye, A growing appreciation for the role of LiF in the solid electrolyte interphase, *Adv. Energy Mater.* 11 (2021) 2100046.
- [38] Y.W. Li, B.H. Yao, K. Yan, Y.G. Zheng, Z. Liang, Y.M. Chiang, Y. Cui, The synergistic effect of lithium polysulfide and lithium nitrate to prevent lithium dendrite growth, *Nat. Commun.* 6 (2015) 1–8.
- [39] J. Jie, L.Y. Liu, L.N. Cong, H.B. Zhang, W. Lu, M.X. Zhang, J. Liu, H.M. Xie, L.Q. Sun, High-performance PVDF-HFP based gel polymer electrolyte with a safe solvent in Li metal polymer battery, *J. Energy Chem.* 49 (2020) 80–88.
- [40] D. Aurbach, E. Pollak, R. Elazari, G. Salitra, C.S. Kelley, J. Affinito, On the surface chemical aspects of very high energy density, rechargeable Li–sulfur batteries, *J. Electrochem. Soc.* 156 (2009) A694–A702.
- [41] F. Ding, W. Xu, G.L. Graff, J. Zhang, M.L. Sushko, X. Chen, Y. Shao, M.H. Engelhard, Z. Nie, J. Xiao, X. Liu, P.V. Sushko, J. Liu, J.G. Zhang, Dendrite-free lithium deposition via self-healing electrostatic shield mechanism, *J. Am. Chem. Soc.* 135 (2013) 4450–4456.
- [42] R. Zhang, X.R. Chen, X. Chen, X.B. Cheng, X.Q. Zhang, C. Yan, Q. Zhang, Lithophilic sites in doped graphene guide uniform lithium nucleation for dendrite-free lithium metal anodes, *Angew. Chem. Int. Ed.* 56 (2017) 7764–7768.